CHAPTER 3

BISTATIC SPECULAR SCATTERING MEASUREMENTS FOR THE ESTIMATION OF RICE CROP GROWTH VARIABLES USING FUZZY INFERENCE SYSTEM AT X-, C-, AND L-BANDS

3.1 INTRODUCTION

Rice in India contributes 20% of the global production (Kumar et al. 2016). It is one of the staple food grains in India and around the world. Hence, timely, accurate, and reliable monitoring of rice crop is essential for better yield and sustainable food security. Crop growth parameters provide crucial information about its health and yield forecasting (Brisco et al. 2014). The monitoring of crop growth parameters at different stages is a time consuming process. Therefore, it is needed to adopt an advanced and robust approach for effective and timely monitoring of crop/vegetation.

Remote sensing techniques have been proven as a potential way to observe, estimate, and monitor the critical biophysical parameters and its characteristics over large and inaccessible areas. Rice crop is mainly cultivated in tropical monsoon season (Chakraborty et al. 2005). The frequent and dense cloud cover during this season hampers the data acquisition using optical remote sensing. Therefore, microwave remote sensing, with its all-weather imaging capabilities, becomes an important and potential technique, especially for paddy rice monitoring (Oh et al. 2009). The estimation of crop growth parameters have been reported by using ground-based scatterometer system (Bouman 1991; Prevot et al. 1993a; Prasad 2011; Kim et al. 2013), air-borne system (Prevot et al. 1993b; Taconet et al. 1994; Macelloni et al. 2001) and space-borne system (Wegmuller and Werner 1997; Blaes and Defourny 2003; Hosseini et al. 2015; Fieuzal and Baup 2016) for its monitoring. Synthetic aperture radar (SAR) data have been used for mapping, monitoring and acreage estimation office crop in

different regions across the world (Toan et al. 1997; Shao et al. 2001; Panigrahy et al. 2002; Yang et al. 2016; Mishra et al. 2017).

The ground-based scatterometer was developed to study the relationship between the backscattering coefficients with the rice crop growth parameters at different microwave bands in full polarimetric modes. Kim et al. (2000) studied the backscattering measurement of rice crop using ground-based scatterometer at X-band for HH-, VV-, and HV-polarizations and showed that an early peak in backscattering coefficient was observed with the plant height. The early peak in the backscattering coefficient was attributed to an increase in random scattering and attenuation by leaves at a higher frequency. Lim et al. (2008) studied the temporal backscattering response of rice crop using ground-based scatterometer at C-band with HH-, HV-, VV-, and HV- polarizations for the range of incidence angle 10°-60° and measured backscattering coefficient was compared with that obtained from the RADARSAT-1 data. Kim et al. (2009) estimated the paddy rice growth parameters at X-, C-, and L-bands by polarimetric scatterometer using second order polynomial regression analysis for the best-correlated rice growth parameters. Kim et al. (2013) continuously monitored the rice crop with a stable ground-based scatterometer system at X-, C-, and L-bands frequencies for a 40° fixed angle to avoid the error due to repositioning adjustment of the scatterometer. In this study, the backscattering coefficients were found highest at L-band, whereas lowest at X-band and the correlation coefficient between the backscattering coefficient with different crop growth parameters were computed at these bands. Inoue et al. (2002) investigated the season-long daily backscattering measurement of the paddy rice field at Ka-, Ku-, X-, C-, and L-bands frequencies for different polarizations and incidence angles. They showed that the best correlation was found for leaf area index (LAI) at C-band for HH- and cross-polarization, whereas biomass was found the best correlated at L-band for HH-and cross-polarization. The

higher frequency band was found poorly correlated with LAI and biomass. These higher frequency bands were found highly correlated with the weight of heads of the rice crop.

Till date, the developed models and experimental researches on vegetation have been focused only in the backscattering direction i.e. monostatic configuration. The monostatic configuration has no capability to acquire multidimensional information on land surface features because the transmitter and receiver are placed at the same position for acquiring monostatic scatterometer measurements. Therefore, the bistatic configuration based radar system, including transmitting and receiving antennas placed in opposite directions, is needed to obtain the multidimensional information about any object on the land surface. It provides additional information about the land surface features due to the diversity of geometry provided by it as compared to the monostatic configuration (Liang et al. 2005). Therefore, researchers have started to study the bistatic scattering mechanism of land surface features. In the current past, the researchers simulated the bistatic scattering coefficient by solving the MIMICS radiative transfer theory and electromagnetic scattering/emission model for vegetation and land surface features. Liang et al. (2005) developed the bistatic scattering radiative transfer model called BI-MIMICS for forest canopy using MIMICS for backscattering. The results of the developed model were simulated for different incidence angle, azimuth angle, and biomass at X-, C-, and L-bands for different polarizations. Zhang and Wu (2016) developed the microwave bistatic scattering model for vegetation using first order radiative transfer theory by adopting the MIMICS model for forest canopy into the agricultural context and simulated the results for wheat and soybean crops at L- and C-bands for different incidence angle, azimuth angle, and crop growth parameters. Ferrazzoli et al. (2000) modeled and simulated the bistatic specular scattering coefficients using electromagnetic scattering and emission theory for the surface covered with sunflower vegetation. In this study, it is reported that the bistatic specular scattering coefficient did not

saturate with biomass, unlike the backscattering coefficient, which shows the saturation effect with the biomass. These simulated results showed a higher sensitivity of vegetation parameters to the bistatic specular scattering coefficient than the backscattering coefficient.

However, very limited experimental results in bistatic scattering configuration for crop/vegetation monitoring have been reported, although its major focus has been in soil moisture and surface roughness study (Nashashibi and Ulaby 2007; Brogioni et al. 2010; Mittal and Singh 2010; Johnson and Quellette 2014). Therefore, the bistatic scatterometer measurements were conducted to obtain the insights about bistatic scattering mechanism of vegetated fields in specular direction ($\phi = 0$) at X-, C-, and L-bands for HH-, VV- and HV-polarizations in the incidence angle ranging from 10°- 60°. The response of bistatic specular scattering coefficients (σ^0) of the rice crop with different crop growth parameters were analyzed at different growth stages for the various angle of incidence, polarization, and microwave frequencies. The correlation analysis between σ^0 and rice crop growth parameters were carried out to select the optimum angle of incidence, polarization, and frequency of the bistatic scatterometer system for the estimation of crop growth parameters.

The accurate estimation of crop growth parameters depends on the quality of data acquired during bistatic scatterometer measurements. Since the bistatic scattering coefficients depend upon the several system parameters and crop growth variables. It further involves very complex mathematical expressions for the computation of the bistatic scattering coefficient (Ferrazzoli et al. 2000; Liang et al. 2005; Zhang and Wu 2016). Therefore, the inversion of these models is a computationally complex and tedious task for the estimation of crop growth parameters. Therefore, a robust and less complex technique is required for the estimation of crop parameters at various growth stages. To overcome the complex computational task, machine learning techniques are being extensively used in scientific and engineering research. The machine learning techniques include artificial neural network

(ANN), fuzzy logic (FL), genetic algorithm (GA), and support vector machine (SVM). The ANN, SVM, and GA have been successfully applied in the field of agriculture for the estimation and classification using remote sensing data (Smith 1993; Fang et al. 2003; Murthy et al. 2003; Jiang et al. 2004; Durbha et al. 2007; Dixon and Candade 2008; Mathur and Foody 2008; Tseng et al. 2008; Kumar et al. 2015, 2017). However, the fuzzy logic inference system is yet to be investigated in detail for the estimation of crop growth parameters using remote sensing data. Therefore, in the present study, the subtractive clustering based fuzzy inference system (S-FIS) was used for the estimation of crop growth parameters at X-, C- and L-bands for HH-, VV-, and HV-polarizations. The performance of the developed S-FIS algorithm was also evaluated by calculating the root mean square error (RMSE) between the observed and estimated values of the rice crop growth parameters.

3.2 EXPERIMENTAL DETAILS

An outdoor rice crop-bed was specially prepared besides the Department of Physics, IIT (BHU), Varanasi, India, for the bistatic specular scatterometer measurements at various growth stages of the crop. The specifications of the bistatic scatterometer system are summarized in Chapter 2. The rice seeds of Rajendra Kasturi variety were sown in a nursery on 8 July 2016. After 30 days, the rice seedlings were transplanted on 7 August 2016 at the measurement site. The bistatic specular scatterometer measurements were carried out from 26 August 2016 to 09 November 2016 at the interval of 15 days before the rice plants were harvested on 14 November 2016. The rice seedlings were transplanted over an area of 10 × 10 m^2 with a spacing of 20 cm between the row and around 15 cm in a column. After transplanting, the field was irrigated as and when required to keep the depth of water about 5 cm from the soil surface of the field until the maturity stage of the crop was attained. The rice crop growth parameters were measured on the same day of bistatic specular scatterometer measurements at six different growth stages. The detailed procedure for the measurement

of crop growth parameters (FBm, LAI, PH, and VWC) of the rice crop at its various growth stages is given in Chapter 2. Since the rice crop cluster can be counted in the crop-bed, therefore, Equations (2.14) and (2.15) given in Chapter 2 were used for the computation of FBm and VWC, respectively.

3.1 METHODS

3.1.1 Brief description of fuzzy inference system (FIS)

The formulation for the mapping from a given input data to the desired output data using fuzzy logic is called fuzzy inference. Fuzzy inference system consists of membership functions, logical operations (AND, OR), and if-then rules. A membership function is a curve that defines the input data (a crisp number) between the values 0 and 1. In the fuzzy inference system, the first step is to take the input data and determine the degree between the values 0 to 1 via membership functions. These components are used in five steps on the input and output data for the fuzzy inference. These five steps are to (i) fuzzify the input (ii) apply the fuzzy operator (AND or OR) in the antecedent (iii) implicate the antecedent to consequent (iv) aggregate all the consequent through the rules and (v) defuzzify the aggregate output to find one single number output (Zadeh 1965; Tagaki and Sugeno 1985).

3.1.2 Subtractive based clustering

The clustering of numerical data is done for grouping the data having some common features. The clustering helps in representing the system's behaviour concisely. Subtractive based clustering has been done for the basis of fuzzy model identification (Chiu 1994). In this method of clustering, each data point in the data sets is considered as a potential cluster center. The measure of the potential of every data point x_i is defined by

$$\mathrm{P}_i = \sum_{j=1}^{n} e^{-\alpha \|x_j - x_i\|^2} \tag{3.3}$$

Where $\alpha = \frac{4}{{r_a}^2}$ and r_a is a positive constant called as potential radius defining the neighbourhood point in the data sets. The data points within this radius have a high effect on the potential, whereas the data points outside this radius have less effect on the potential.

The data point having the highest potential value is chosen as a first cluster center after calculating the potential value of every data point. If x_1^* is the location of the first cluster center and P_1^* is its potential value, then the revision of potential value of every data point is done by the following formula

$$P_i \leftarrow P_i - P_1^* e^{-\beta \|x_j - x_i\|^2} \tag{3.4}$$

Where $\beta = \frac{4}{{r_b}^2}$ and r_b is a positive constant greater than r_a. It defines the radius corresponding to the low potential value of the neighbourhood data point.

After evaluating the potential value of all the data points using the above formula, the data point having the higher potential value is selected as a second cluster center. This process is repeated until all the possible cluster centers are obtained. Every k_{th} cluster center is processed by the following conditions (Yager and Filev 1994):

If $P_k^* > \overline{\varepsilon}\, P_1^*$, then x_k^* is selected as the cluster center and clustering is continued otherwise if $P_k^* < \underline{\varepsilon}\, P_1^*$, then x_k^* is rejected as cluster center and clustering is ended. Where $\overline{\varepsilon}$ and $\underline{\varepsilon}$ are the two fractional threshold parameters for the potential values which decide to accept or reject the cluster centers, respectively.

There is another way of testing, let d_{min} be the shortest distance between x_k^* and all the earlier obtained cluster centers:

If $\frac{d_{min}}{r_a} + \frac{P_k^*}{P_1^*} \geq 1$, then x_k^* is selected as the cluster center and clustering is continued otherwise x_k^* is set to the 0 value potential and clustering is ended.

After the cluster estimation of data sets, each cluster center in the data sets defines the system behaviour concisely, since the cluster center of cluster describes the data group by a

single rule. Hence, each cluster center is used as the basis of a rule that describes the system behaviour. If x_i^* is the cluster center, then the degree of membership value (μ_i) of an input data *x* for any rule is given by

$$\mu_i = e^{-\alpha\|x-x_i^*\|^2} \tag{3.5}$$

Where α is defined by the Equation (3.3). Then, the output *y* is calculated by

$$y = \frac{\sum_{i=1}^{c} \mu_i y_i^*}{\sum_{i=1}^{c} \mu_i} \tag{3.6}$$

Where y_i^* and c are the cluster center in the output data and the total number of clusters generated in the data sets, respectively.

In the present study, the ***genfis2*** function of the fuzzy logic toolbox in MATLAB was used to develop the S-FIS algorithm for the estimation of rice crop growth parameters.

3.4 RESULTS AND DISCUSSION

Figure 3.1 shows the temporal variation of the rice crop growth parameters under study. All the rice crop growth parameters were found increasing with its age up to 80 days after transplanting the seedling. After 80 days, the rice crop started to attain its maturity stage (drying stage). Therefore, after attaining the maturity stage, the rice crop growth parameters were started to decrease. Figures 3.2-3.10 show the temporal variation of σ^o in the angular range of incidence angle 20°- 60°at X-, C-, and L-bands for HH-, VV-, and HV-polarizations, respectively at different growth stages of rice crop. The values of σ^o were found decreasing with the age of crop at HH- and VV-polarizations for all the three bands while it was found increasing at HV-polarization. Since the main contribution for bistatic specular scattering at HH- and VV-polarizations is the coherent component of microwave reflected from the water background beneath the crop in the specular direction. Therefore, the decreasing trend in HH- and VV-polarizations at all three bands are due to the attenuation of the coherent components of the incident microwave as well as the screening of the water background beneath the crop components caused by the increasing rice crop growth parameters in the specular direction.

While the increasing trends at HV-polarization are because of depolarization of the incident microwave caused by the increasing roughness/randomness of crop canopy with the growth stages. At the older stage i.e. after the maturity stage (drying stage) of rice crops, the crop growth parameters started to decrease. Therefore, the attenuation introduced to the coherent component was found lower at the older stage due to the low quenching effect from the crop having lower vegetation water content and plant height. Therefore, the penetration depth of the incident microwave into the crop canopy increases up to the water background beneath the crop. This caused to increase in the reflected coherent component from the water background beneath the crop, acting as a smooth surface, in the form of enhanced bistatic specular scattering coefficient at the older stage of the crop (Ferrazzoli et al. 2000). Therefore, during the maturity stage, σ^0 was started increasing at HH- and VV-polarizations and decreasing at HV-polarization for all the X-, C-, and L-bands due to the decrease of vegetation moisture content and crop growth parameters after attaining the maturity stage of the rice crop.

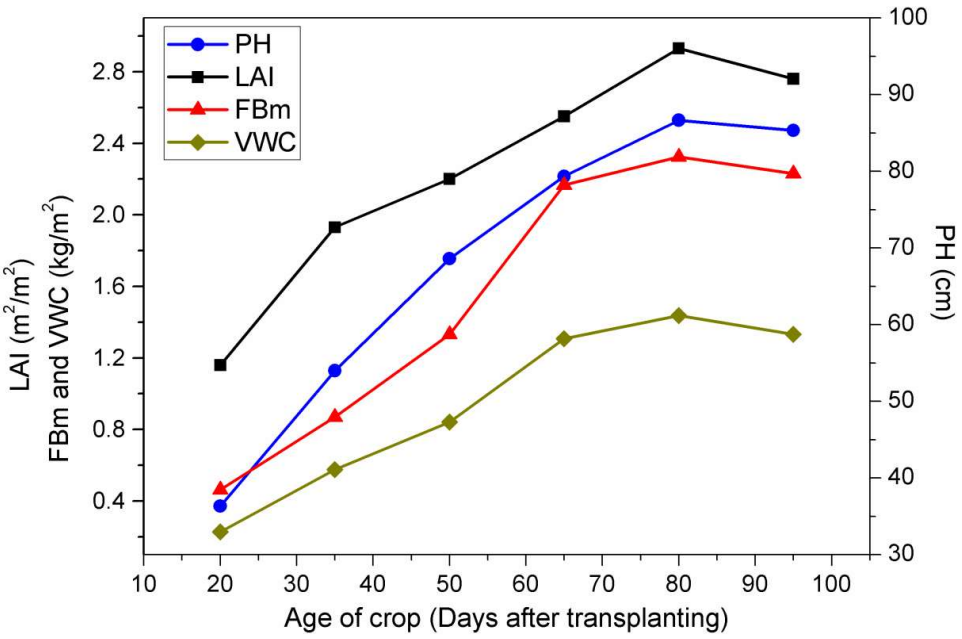

Figure 3.1 Temporal variation of rice crop growth parameters

The values of σ^o at C-band were found to be higher as compared to X- and L-bands for HH- and VV-polarizations. However, the difference between the values of σ^o at C-band and X-bands was found to decrease at higher angle of incidence. The highest value of σ^o at C-band for HH- and VV-polarizations may be attributed to both the direct crop canopy and water backgrounds beneath the crop are as the dominant scattering components. While at X-band, only direct crop canopy scattering was found dominant, and water background beneath the crop scattering showed low contribution because of higher attenuation caused by the rice crop canopy. Since, as the frequency increases, the scattering from the water background beneath the crop decreases significantly due to attenuation (absorption) of the incident microwave frequency caused by its canopy present over the water background. Thus, the direct crop canopy scattering component becomes strongest at X-band. At L-band, the only dominant scattering component is from the water background beneath the crop due to its higher penetration into the rice crop. There is comparatively large attenuation at L-band caused by the higher penetration into the rice crop, and volume scattering occurred within the crop canopy resulting in low σ^o values. Therefore, the values of σ^o were found low at L-band as compared to C- and X-bands. On the other hand, only direct crop canopy scattering was found dominant at cross-polarization HV for the incident microwave frequencies. Hence, at cross-polarization HV, the values of σ^o were found highest for X-band, followed by C-and L-band frequencies (Liang et al. 2005; Zhang and Wu 2016). In addition, the values of σ^o were found lower at VV-polarization due to significant interaction of the microwave frequencies with the vertical stalks of the rice crop, as a vertically oriented lossy dielectric cylinders, resulting to attenuation as compared to HH-polarization (Ulaby et al. 1987). Therefore, the vertical stalks of the rice crop caused more attenuation at VV-polarizations for all the X-, C-, and L-bands.

The sensitivity of crop growth parameters with the σ^o may be defined by the dynamic range of the angular variation of the σ^o in the angular range of incidence angle 20°- 60°. The dynamic range of σ^o was found greater at the older stages than the early growth stages of the rice crop for all three bands at different polarization configurations. When the values of crop growth parameters were small at early stages, the attenuation caused by the crop growth parameters was small, and the contribution from the water background beneath the crop scattering was found dominant. The attenuation caused by the increased rice crop growth parameters and higher path (slant height) in the crop at higher incidence angle led to higher dynamic range of σ^o at its later growth stages. Thus, the difference in the dynamic range of σ^o at different crop growth stages may be helpful to differentiate the early and later growth stages using bistatic specular scatterometer measurements.

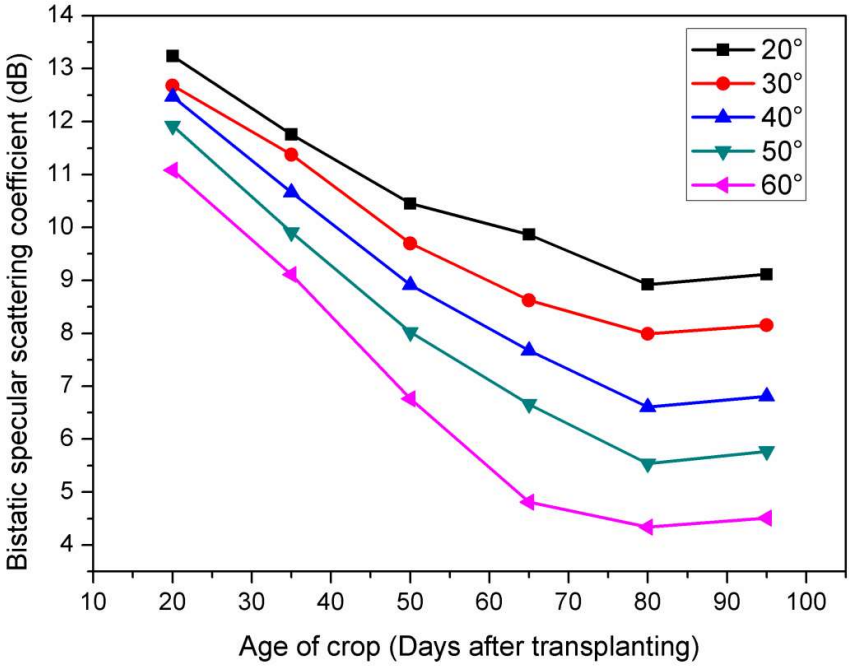

Figure 3.2 Temporal variation of σ^0 at X-band for HH-polarization

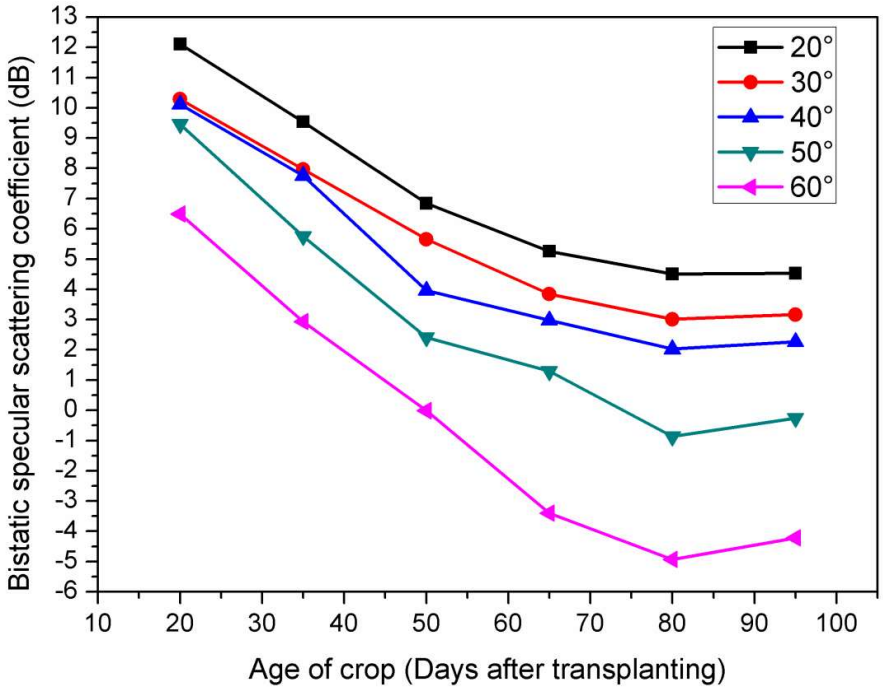

Figure 3.3 Temporal variation of σ^0 at X-band for VV-polarization

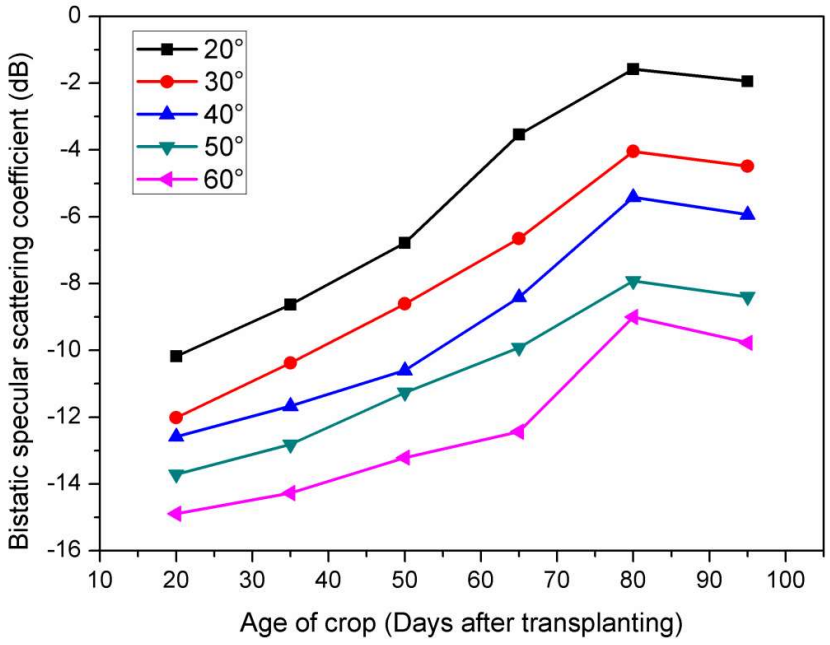

Figure 3.4 Temporal variation of σ^0 at X-band for HV-polarization

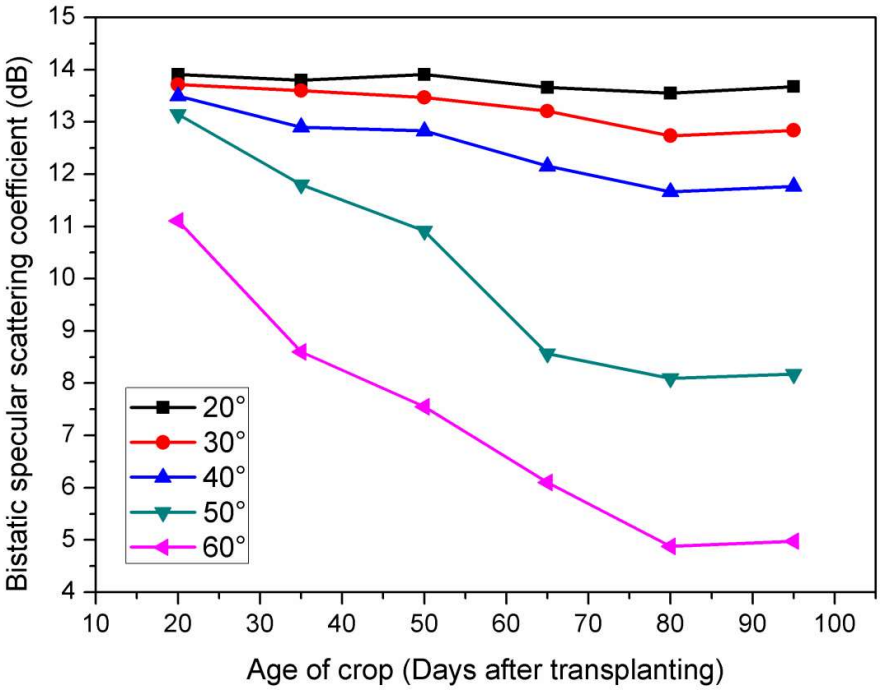

Figure 3.5 Temporal variation of σ^0 at C-band for HH-polarization

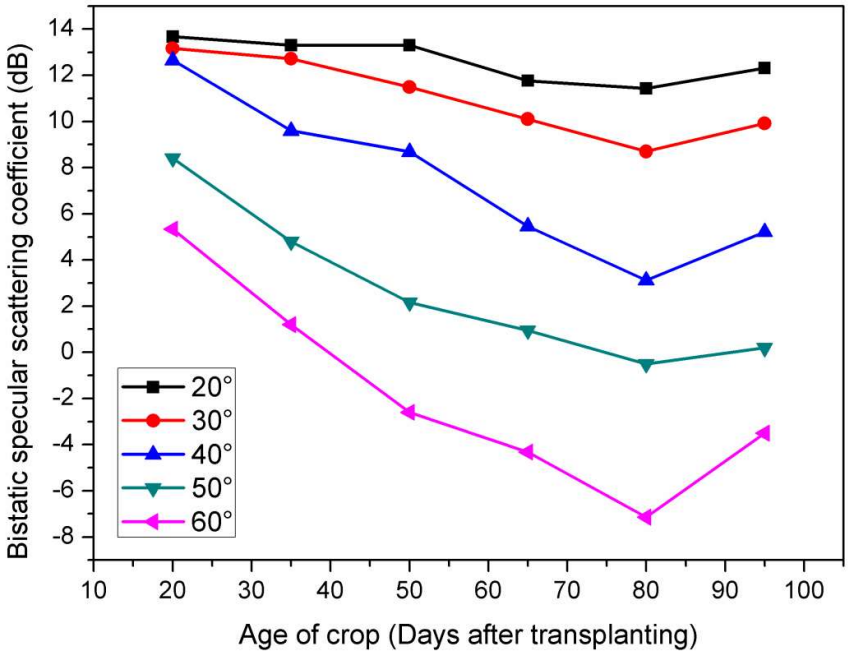

Figure 3.6 Temporal variation of σ^0 at C-band for VV-polarization

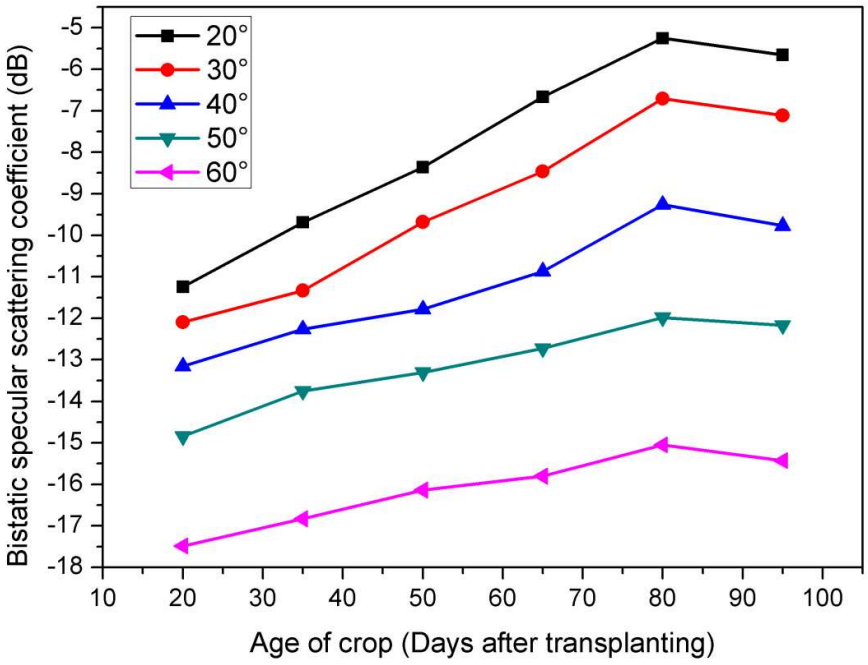

Figure 3.7 Temporal variation of σ^0 at C-band for HV-polarization

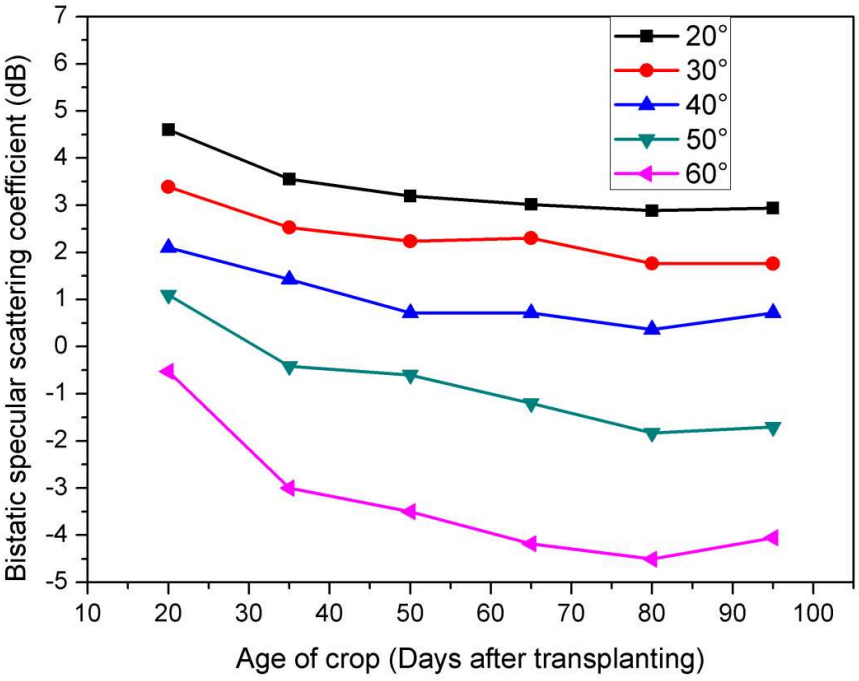

Figure 3.8 Temporal variation of σ^0 at L-band for HH-polarization

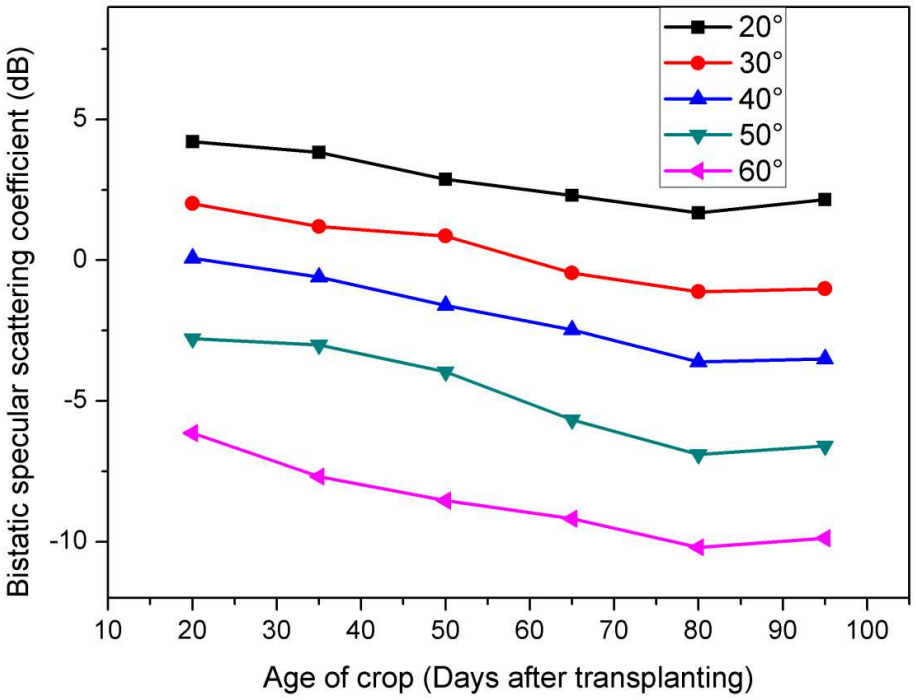

Figure 3.9 Temporal variation of σ^0 at L-band for VV-polarization

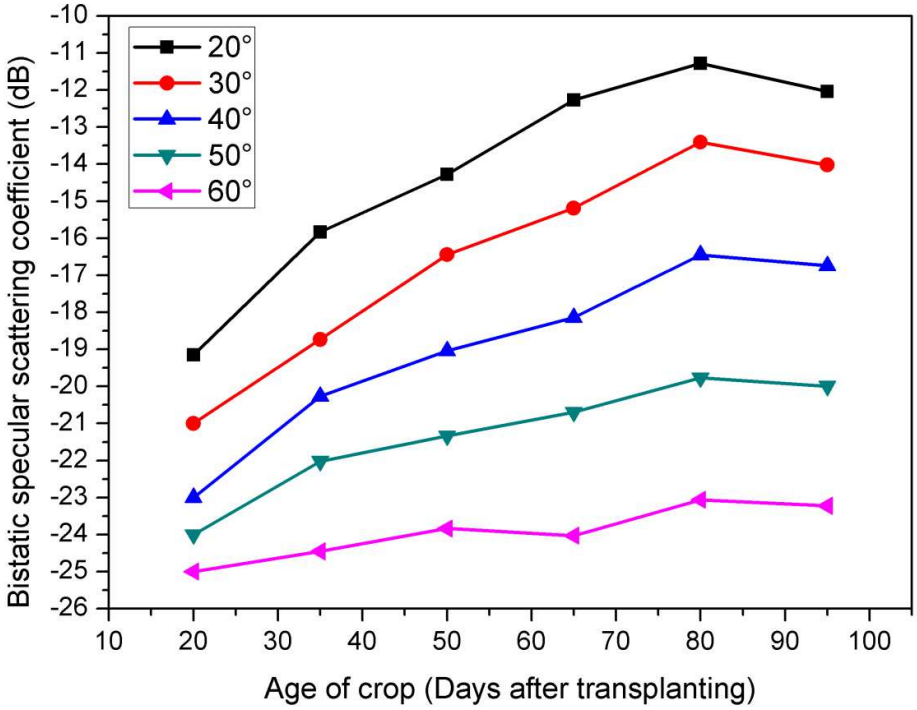

Figure 3.10 Temporal variation of σ^0 at L-band for HV-polarization

The scattering behaviour of the microwave with the crop growth parameters can also be studied from the flatness/steepness of the angular variation of σ^0 at different growth stages using scatterometer configured at multi-polarizations (HH, VV, and HV) and multi-frequency bands (X, C, and L) (Ferrazzoli et al. 2000). In Figures 3.5 and 3.6, the variation of σ^0 with the age was found more flatter at incidence angles 20°, 30° and 40° for HH-polarization and 20°, 30° for VV-polarization at C-band. Whereas, the variation of σ^0 with the age was found steeper at 50° and 60° angle of incidence for HH-polarization and 40°, 50° and 60° incidence angle for VV-polarization. This anomalous behaviour of σ^0 with the age of the rice crop can also be described on the basis of the dominant contribution from both the direct crop canopy and water background beneath the crop scattering at C-band. The contributions to σ^0 from the direct crop canopy as well as its water background beneath the crop scattering components were found significant at 20°, 30° and 40° for HH-polarization and at 20°, 30° for VV-polarization. Whereas, the contribution to σ^0 from the direct crop canopy scattering component became dominant as compared to its water background beneath the crop scattering components at 50° and 60° for HH-polarization and at 40°, 50° and 60° for VV-polarization. At lower incident angle, the water background beneath the crop scattering components was found larger due to the smaller slant path of the microwave through the crop canopy. Thus, both the direct rice canopy (vegetation scattering) and the water background beneath the crop scattering components were found dominant at lower incident angle leading to almost flat curve of σ^0 with the age of crop. At higher angle of incidence, the water background beneath the crop scattering component was found low due to attenuation caused by increased slant path in the crop canopy medium (Ulaby and Jedlicka 1984; Ulaby et al. 1987). Therefore, there is a significant decrease in the water background beneath the crop scattering component at higher angle of incidence and hence, only direct crop canopy

(vegetation scattering) remains the dominant scattering component. Therefore, the steeper variation of σ^0 with the age of crop was observed at higher angle of incidence.

The correlation analysis was carried out between the σ^0 and rice crop growth parameters to determine the optimum angle of incidence and polarization at X-, C-, and L-bands for the estimation of growth variables using subtractive clustering based fuzzy inference system (S-FIS). The highest coefficient of determination between σ^0 and rice crop growth parameters were found at 40° incidence angle for all the three microwave bands used in the present study. At X-band, the highest coefficient of determination between σ^0 and crop growth parameters were found for HH-polarization as compared to VV- and HV-polarizations. At C-band, the second highest coefficient of determination was found for VV-polarizations as compared to HH- and HV-polarizations. At L-band, the third highest coefficient of determination was found for VV-polarization as compared to HH- and HV-polarizations. Thus, the lowest coefficient of determination was found at L-band as compared to X- and C-bands. The highest correlation at X-band and the lowest correlation at L-band with growth parameters imply that higher frequency strongly interacts with the crop growth parameters as compared to lower frequency bands. The crop growth variable VWC was found to have the highest coefficient of determination at X-and C-bands. FBm was found to have a slightly higher coefficient of determination as compared to VWC at L-band. PH was found to have the lowest coefficient of determination among three bands under the investigation. Thus, the correlation analysis showed high correlation at 40° angle of incidence between σ^0 and crop growth parameters, as summarized in Table 3.1.

Table 3.1 Coefficient of determination (R^2) between the bistatic specular scattering coefficients at 40° incidence angle at X-, C-, and L- bands for HH-, VV-, and HV-polarizations with the rice crop growth parameters

Crop growth parameters	Coefficient of determination (R^2)								
	X - band			C - band			L - band		
	HH-pol	VV-pol	HV-pol	HH-pol	VV-pol	HV-pol	HH-pol	VV-pol	HV-pol
FBm	0.964	0.920	0.902	0.947	0.952	0.908	0.815	0.951	0.912
LAI	0.976	0.935	0.857	0.941	0.960	0.914	0.916	0.925	0.895
PH	0.956	0.939	0.859	0.925	0.939	0.899	0.914	0.922	0.902
VWC	0.978	0.937	0.889	0.951	0.970	0.912	0.861	0.949	0.941

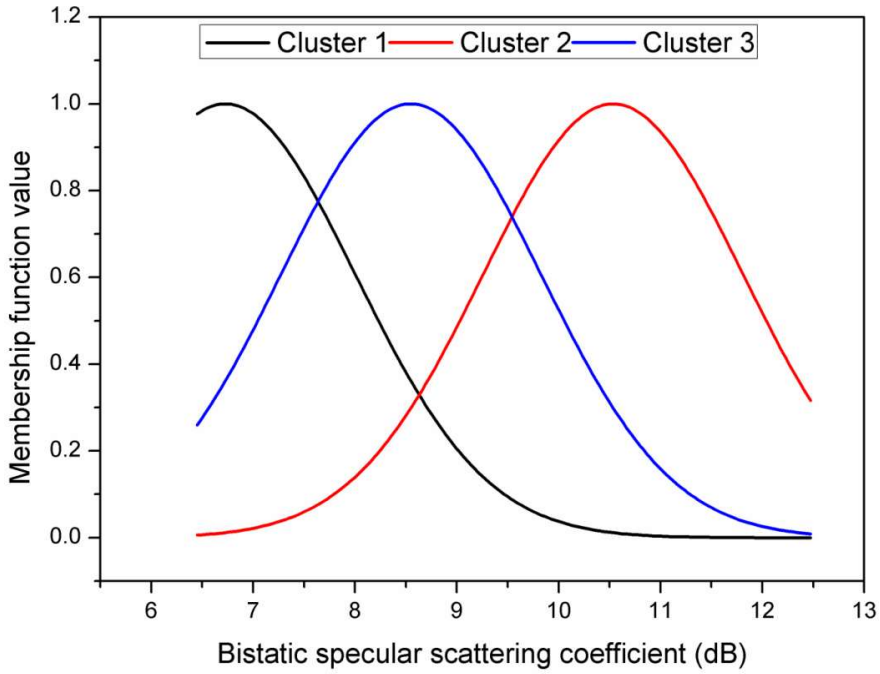

Figure 3.11 Membership function plot for HH-polarization at X-band for FBm

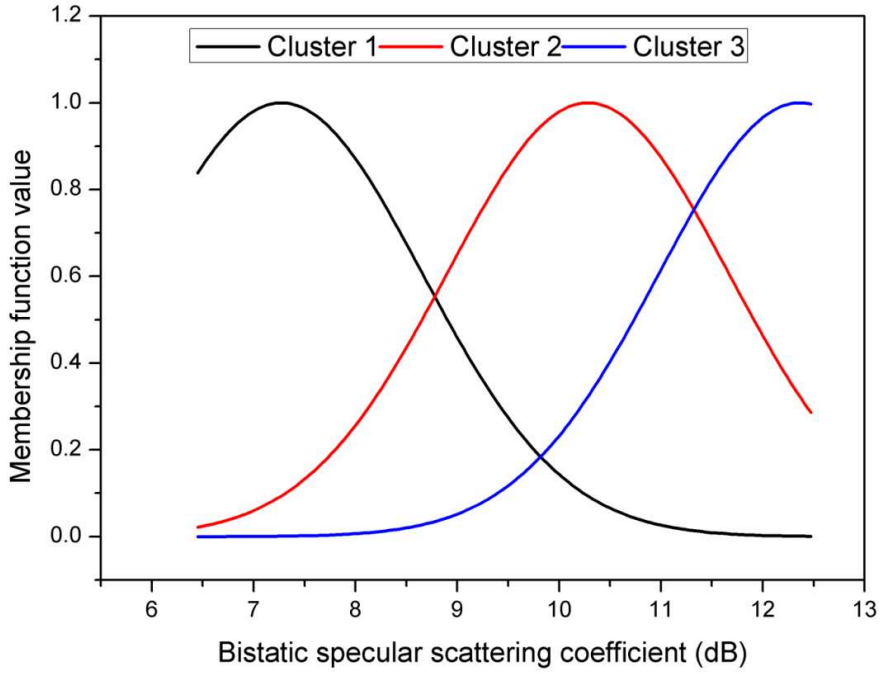

Figure 3.12 Membership function plot for HH-polarization at X-band for LAI

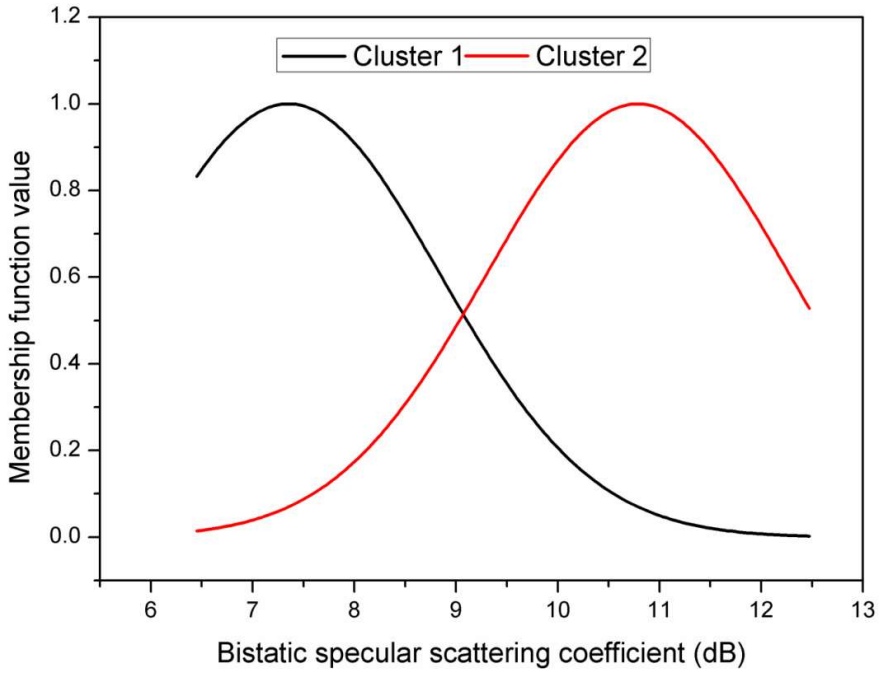

Figure 3.13 Membership function plot for HH-polarization at X-band for PH

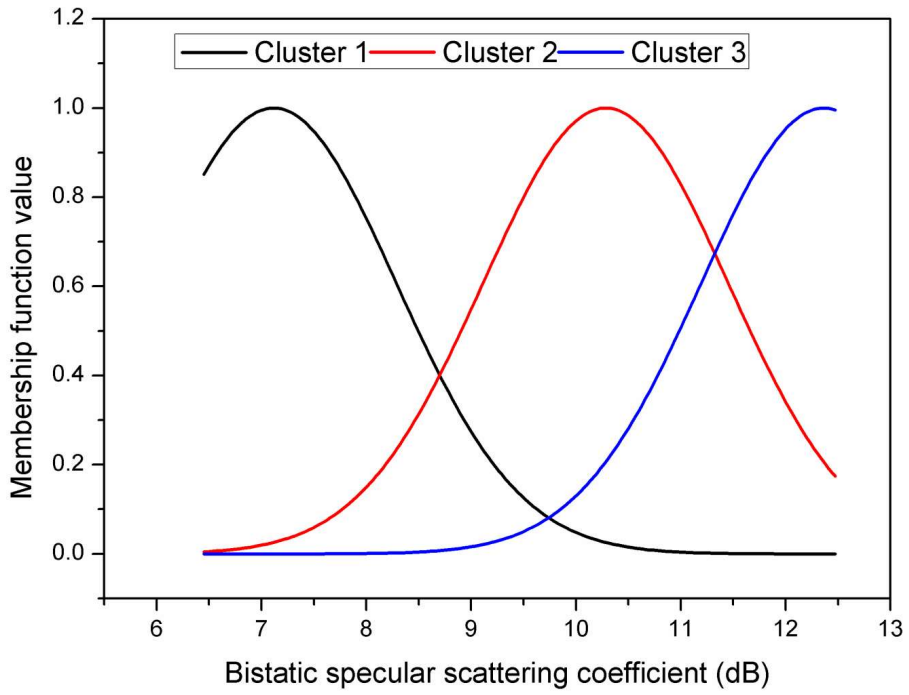

Figure 3.14 Membership function plot for HH-polarization at X-band for VWC

Therefore, the data sets consisting of σ^0 and crop growth parameters at 40° incidence angle for HH-polarizations at X-band were considered for the estimation of rice crop growth parameters using the S-FIS algorithm. For this, the interpolation of the data sets corresponding to 20 to 95 days was done to generate additional 76 days data sets at the interval of one day for the estimation of the crop growth parameters. The cubic spline interpolatin method was used to perform the interpolation of data sets using Origin 8.1 to get the daily interval data from the longer interval data in this thesis. Spline interpolation is often preffered because the interpolation error can be made small even using low degree polynomials for the spline. From these 76 data sets, 57 data sets were used for the training of developed S-FIS algorithm. The remaining data sets at the interval of 3 days were used for the testing of the developed S-FIS algorithm. The σ^0 was taken as input, and the crop growth parameters, namely FBm, LAI, PH, and VWC, were taken as output data sets for developing the fuzzy inference system.

The optimum number of MF should be chosen for generating the number of rules between input and output data sets. Since, larger number of MF will result larger number of fuzzy rules leading to over fitting the training and testing data while the smaller number of MF generates smaller number of fuzzy rules leading to courser model. Therefore, optimum number of MF should be chosen for the good balance between the number of fuzzy rules and RMSE values due to larger number of MF for the partition of the input data sets. In the S-FIS model setting, the optimum value of the cluster radius was chosen in order to have a good balance between the number of fuzzy rules and RMSE so as to get estimated crop growth parameters much closer to the observed values. The optimum value of cluster radius was chosen by training the model using the radii value between 0 to 1 in step of 0.05 by trial-error method and calculating the RMSE between the observed and estimated values at these radii values (Chiu 1994). The optimum value of cluster radius and hence the optimal model was chosen where the RMSE started to diverge during training and testing of S-FIS model.

Table 3.2 shows the values of RMSE between the estimated and observed crop growth parameters for the optimized value of the cluster radius and various other parameters of the S-FIS algorithm. The lowest RMSE value for the estimation of LAI was found at X-band for HH-polarization as compared to FBm, PH, and VWC. The optimum value of the cluster radius and corresponding generated number of membership functions were found to be 0.65 and 3, respectively. Therefore, the estimation of LAI would be better at X-band for HH-polarization using the S-FIS algorithm. Figures 3.11-3.14 show curves for the membership function (MF), describing the degree of fulfillment (membership value) of μ_i for each rule as a function of $\sigma°$, for X-bands at HH-polarization for different crop growth parameters. The estimated values using the developed fuzzy algorithm were found very close to the observed values of all the rice crop growth parameters. Figures 3.15-3.18 show the high performance of the developed S-FIS algorithm indicated by low RMSE value for the

estimation of crop growth parameters for the training and testing. Its high potential is also evident from Tables 3.2 indicating minimum values of RMSE for the estimation of all the rice crop growth parameters during the training and testing of the developed S-FIS algorithm.

Table 3.2 The optimum values of various parameters of S-FIS algorithm at X-band for HH-polarization

Crop growth parameters	FBm	LAI	PH	VWC
Optimum value of cluster radius	0.6	0.65	0.7	0.55
Number of cluster generated	3	3	2	3
Number of fuzzy rules	3	3	2	3
Number of membership functions	3	3	2	3
RMSE (training)	0.0236	0.0169	0.6160	0.0292
RMSE (testing)	0.0291	0.0223	0.6430	0.0308

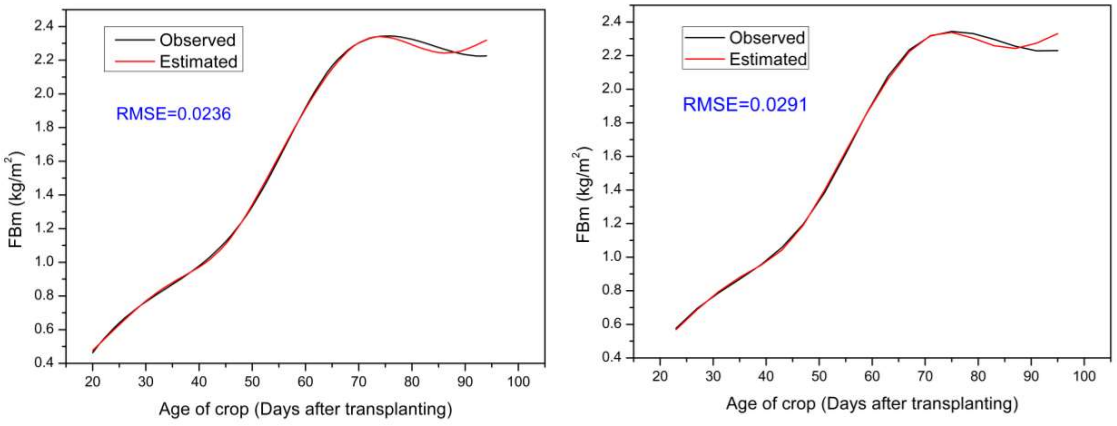

(a) **(b)**

Figure 3.15 Fuzzy algorithm performance for the estimation of FBm at 40° angle of incidence for HH-polarization at X-band for (a) training and (b) testing

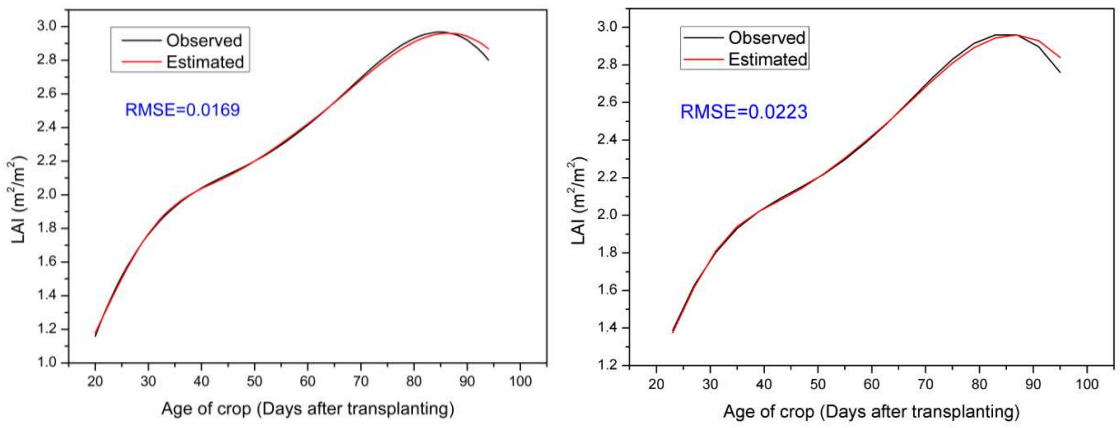

(a) **(b)**

Figure 3.16 Fuzzy algorithm performance for the estimation of LAI at 40° angle of incidence for HH-polarization at X-band for (a) training and (b) testing

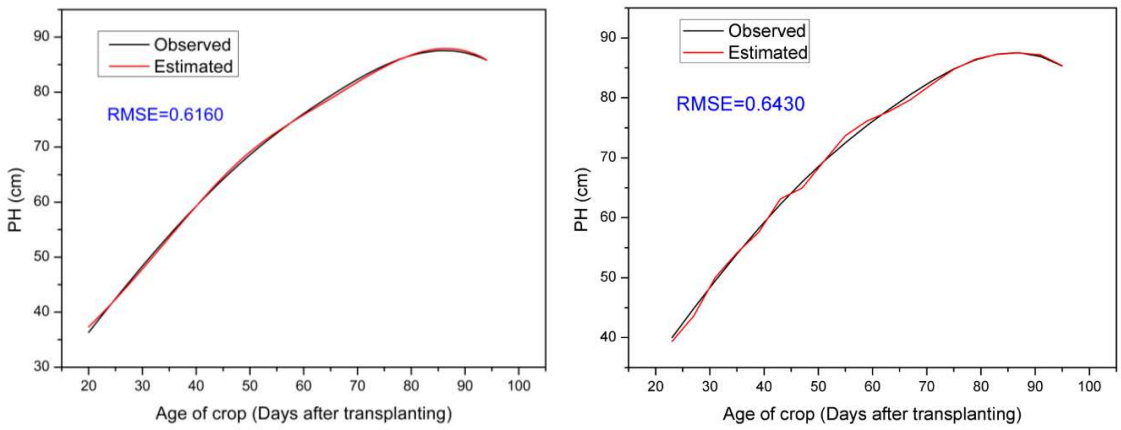

(a) **(b)**

Figure 3.17 Fuzzy algorithm performance for the estimation of PH at 40° angle of incidence for HH-polarization at X-band for (a) training and (b) testing

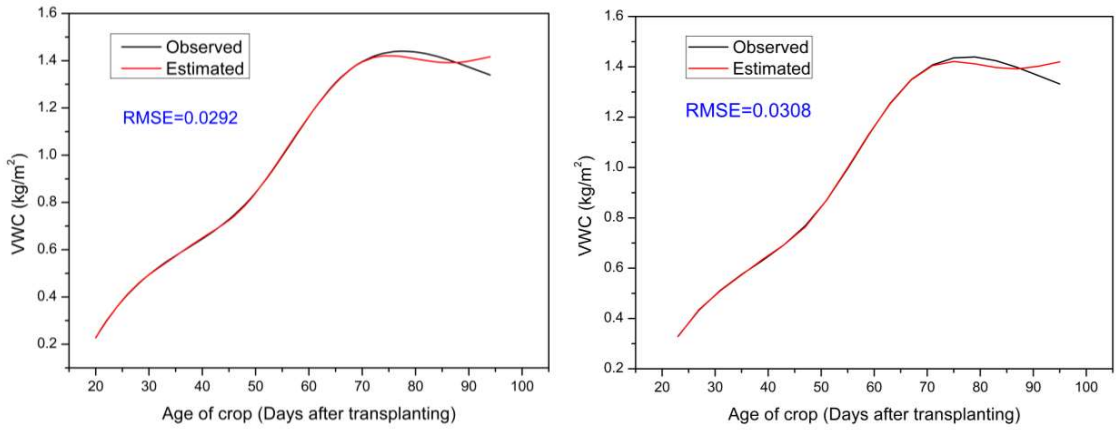

(a) **(b)**

Figure 3.18 Fuzzy algorithm performance for the estimation of VWC at 40° angle of incidence for HH-polarization at X-band for (a) training and (b) testing

3.5 CONCLUSIONS

The values of σ^0 were found to decrease with the age of rice crop until the maturity stage was attained at HH- and VV-polarizations. After the maturity stage, σ^0 values were started to increase slightly due to the decrease in crop growth parameters. The opposite trend was observed for the values of σ^0 at HV-polarization. The highest values of σ^0 were found at C-band as compared to X- and L-bands for HH- and VV-polarizations because of the dominant contributions from both the direct crop canopy and water background beneath the crop scattering. At lower incidence angle, both the direct crop canopy and water background beneath the crop scattering led to the significant values of σ^0 while at higher incidence angle, the dominant contribution was observed only from the direct crop canopy at C-band. At 40° angle of incidence, σ^0 was found highly correlated with all the crop growth parameters for HH-polarization at X-band and for VV-polarization at C- and L-bands. The estimation efficiency of crop growth parameters using the developed S-FIS algorithm for the optimum value of cluster radii was found good. The performance index RMSE showed that the

estimated values of crop growth parameters were very close to the observed values. Therefore, the results of this study for the estimation of rice crop growth parameters may be used to suggest a suitable angle of incidence, polarization, and different microwave bands for the future bistatic radar system to monitor the rice crop fields effectively.